

Nitrogen-Rich Carbon Nitride Network Materials via the Thermal Decomposition of 2,5,8-Triazido-s-Heptazine

Dale R. Miller, James R. Holst, and Edward G. Gillan*

Department of Chemistry and the Optical Science and Technology Center, University of Iowa, Iowa City, Iowa 52242

Received July 13, 2006

This report describes the rapid and slow thermal decomposition of an energetically unstable polycyclic and heterocyclic azide, triazido-s-heptazine (C_6N_{16}), to produce nitrogen-rich CN_x materials ($x > 1.2$). An analysis of gaseous byproducts shows that this large heterocyclic precursor releases primarily N_2 gas during its decomposition. The product composition and its morphology are dependent on the rapidity of the TAH decomposition. The CN_x products are thermally stable to 500 °C and exhibit variations in H and O content dependent on precursor preparation and atmospheric exposure. The rapid decomposition of TAH leads to visibly porous powders, while slow decomposition yields smooth monoliths that are reminiscent of the morphology of the starting polycrystalline powder. IR and NMR spectral similarities between the amorphous CN_x products and several previously reported heptazine molecules and extended heptazine networks supports significant retention of heptazine motif in these amorphous carbon nitride extended materials.

Introduction

The past 20 years have seen a great deal of progress in the field of carbon nitride (CN_x) materials. In large part, this surge in research was due to the theoretical work on β - C_3N_4 ¹ and related polymorphs² that were predicted to have important technological applications as superhard materials. While no reliable reports of single-phase crystalline C_3N_4 materials have been reported, amorphous low-nitrogen-content CN_x films ($x \ll 1$) are used as protective coatings in the magnetic recording industry due to their superior properties of high hardness, low friction, and wear performance compared to traditional carbon coatings.³ In addition, CN_x materials have found application in the areas of low dielectrics, semiconductors, and electron field emission.⁴ Nanoscale CN_x solids have also shown promise as hydrogen and lithium storage materials⁵ and gas sensors.⁶

There are several synthetic approaches toward producing carbon nitride materials, and many involve high-energy, physical techniques that result in nitrogen-poor materials (CN_x where $x < 1$).⁷ Most of the successful synthetic routes that produce nitrogen-rich CN_x materials involve the use of *s*-triazine (C_3N_3) precursors.⁸ While low-nitrogen-content CN_x ($x \ll 1$) powders and films are most likely nitrogen-doped graphite-like (sp^2) or hard carbon (sp^3) structures, nitrogen-rich products (CN_x where $x > 1$) are dominated by disordered, locally conjugated (sp^2 hybridized) C–N network

* To whom correspondence should be addressed. E-mail: edward-gillan@uiowa.edu.

- (1) (a) Liu, A. Y.; Cohen, M. L. *Science* **1989**, *245*, 841. (b) Liu, A. Y.; Cohen, M. L. *Phys. Rev. B* **1990**, *41*, 10727.
- (2) Teter, D. M.; Hemley, R. J. *Science* **1996**, *271*, 53.
- (3) Scharf, T. W.; Ott, R. D.; Yang, D.; Barnard, J. A. *J. Appl. Phys.* **1999**, *85*, 3142.
- (4) (a) Zhong, D.; Liu, S.; Zhang, G.; Wang, E. G. *J. Appl. Phys.* **2001**, *89*, 5939. (b) Sugino, T.; Etou, Y.; Tai, T.; Mori, H. *Appl. Phys. Lett.* **2002**, *80*, 649. (c) Jimenez, I.; Gago, R.; Garcia, M. M.; Albella, J. M. *J. Vac. Sci. Technol. B* **2001**, *19*, 1358.

- (5) (a) Zhong, D. Y.; Zhang, G. Y.; Liu, S.; Wang, E. G.; Wang, Q.; Li, H.; Huang, X. *J. Appl. Phys. Lett.* **2001**, *79*, 3500. (b) Bai, X. D.; Zhong, D.; Zhang, G. Y.; Ma, X. C.; Liu, S.; Wang, E. G.; Chen, Y.; Shaw, D. T. *Appl. Phys. Lett.* **2001**, *79*, 1552.
- (6) Abedinov, N.; Popov, C.; Yordanov, Z.; Rangelow, I. W.; Kulisch, W. *Appl. Phys. A* **2004**, *79*, 531.
- (7) Muhl, S.; Mendez, J. M. *Diamond Relat. Mater.* **1999**, *8*, 1809.
- (8) (a) Kouvetakis, J.; Todd, M.; Wilkens, B.; Bandari, A.; Cave, N. *Chem. Mater.* **1994**, *6*, 811. (b) Zhang, Z.; Leinenweber, K.; Bauer, M.; Garvie, L. A. J.; McMillan, P. F.; Wolf, G. H. *J. Am. Chem. Soc.* **2001**, *123*, 7788. (c) Montigaud, H.; Tanguy, B.; Demazeau, G.; Alves, I.; Birot, M.; Dunogues, J. *Diamond Relat. Mater.* **1999**, *8*, 1707. (d) Lu, Q.; Cao, C.; Li, C.; Zhang, J.; Zhu, H.; Kong, X.; Duan, X. *J. Mater. Chem.* **2003**, *13*, 1241. (e) Khabashesku, V. N.; Zimmerman, J. L.; Margrave, J. L. *Chem. Mater.* **2000**, *12*, 3264. (f) Huynh, M. H. V.; Hiskey, M. A.; Archuleta, J. G.; Roemer, E. L.; Gilardi, R. *Angew. Chem., Int. Ed.* **2004**, *43*, 5658. (g) Guo, Q. X.; Yang, Q.; Yi, C. Q.; Zhu, L.; Xie, Y. *Carbon* **2005**, *43*, 1386. (h) Guo, Q. X.; Xie, Y.; Wang, X. J.; Zhang, S. Y.; Hou, T.; Lv, S. C. *Chem. Commun.* **2004**, *26*. (i) Guo, Q. X.; Yang, Q.; Zhu, L.; Yi, C. Q.; Zhang, S.; Xie, Y. *Solid State Commun.* **2004**, *132*, 369.

structures. These latter materials are more akin to cross-linked covalently bonded polymers and have a pronounced tendency to increase hydrogen content along with increasing nitrogen. Several reviews of CN_x film growth and characterization have appeared recently⁹ and a comprehensive review on CN_x precursor methods carefully outlines the hydrogen content issues with nitrogen-rich carbon nitrides.¹⁰ By virtue of their potentially porous structure and high concentration of Lewis basic nitrogen sites, nitrogen-rich carbon nitrides have potential as coordinatively active and chemically derivatizable extended solid analogues of conjugated molecular C–N structures, such as porphyrins and phthalocyanines, and bipyridines.

Our group has examined energetic triazine precursors and volatile film-forming amino-triazines as precursors for CN_x powder and film growth.¹¹ Recently we embarked on the design of larger polycyclic C–N precursors based on a symmetric *s*-heptazine core (C_6N_7 , also known as tri-*s*-triazine or 1,3,4,7,9,9b-heptaazaphenalene) that mimics a small planar fragment of a nitrogen-substituted graphite layer. We determined the crystal structure of the energetically unstable 2,5,8-triazido-*s*-heptazine (TAH, C_6N_{16}) molecule and presented preliminary data on its thermal decomposition properties.¹² Other groups have studied heptazine-based precursor routes to CN_x structures¹³ and have structurally characterized several heptazine anions and neutral molecules, many of which have potentially useful luminescent emission properties.¹⁴ Recently, heptazine-derived CN_x solids have shown promise as Lewis basic organocatalysts.¹⁵

Experimentally determined optical and structural properties of heptazine molecules are generally consistent with those

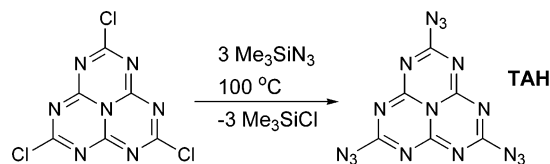


Figure 1. Graphical schematic of triazido-*s*-heptazine (TAH) precursor synthesis.

predicted by recent theory.¹⁶ A common bonding motif followed by all structurally characterized heptazines is that the strongest double bond conjugation exists along the heptazine periphery (~ 1.33 Å C–N bonds) and the central nitrogen lies in the molecular plane, leading to completely planar C_6N_7 cores. It should be noted that most modern synthetic routes to heptazines trace their roots back to the early 1800s, following methods developed by Liebig¹⁷ to produce planar structures that were first correctly predicted by Pauling and crystallographically determined by Leonard.¹⁸

In the research described below, the thermal decomposition of the energetically unstable TAH molecular azide precursor was utilized to generate carbon nitride powders by three different methods. One decomposition method employed rapid heated filament initiation that was successful in our prior CN_x ($x > 1.3$) powder synthesis via trichloromelamine decomposition.^{11d} TAH was also decomposed by either rapid or stepwise heating processes in a stainless-steel autoclave. In all cases, the result was a nitrogen-rich carbon nitride powder with a formula near C_3N_4 exhibiting thermal stability up to 500 °C. Rapid decomposition methods produced porous, spongelike structures, while slow decomposition resulted in faceted structures reminiscent of the microcrystalline precursor powder.

Experimental Section

Thermal Decomposition of 2,5,8-Triazido-*s*-heptazine (TAH).

The synthesis of TAH was reported in detail in our previous work, and a brief synthetic schematic is shown in Figure 1.¹² **Warning:** TAH is a thermally unstable solid and as such must be handled with the same care afforded similar potentially explosive materials. It will deflagrate when hit with a hammer and may release the toxic HN_3 gas when brought in contact with protonic acids. The generation of carbon nitride materials via thermal decomposition of TAH involved three different methods.

Method 1. Inside an argon-atmosphere glovebox, TAH (100 mg, 0.34 mmol) was placed inside a 30 mL Pyrex beaker. The beaker was covered with aluminum foil, and the foil was pierced several times to create a vented container. The beaker/foil assembly was placed in a stainless steel Parr autoclave (model 4750, 110 mL capacity). The system was sealed with a stainless steel headpiece equipped with a 3000 psi pressure gauge, a pressure release valve, and a steel-jacketed, internal thermocouple. Rapid decomposition was achieved using a custom Glas-Col heating mantle to reach an

- (9) (a) Hellgren, N.; Guo, J. H.; Luo, Y.; Sathe, C.; Agui, A.; Kashtanov, S.; Nordgren, J.; Agren, H.; Sundgren, J. E. *Thin Solid Films* **2005**, *471*, 19. (b) Rodil, S. E. *Diamond Relat. Mater.* **2005**, *14*, 1262. (c) Ronning, C.; Feldermann, H.; Merk, R.; Hofsass, H.; Reinke, P.; Thiele, J.-U. *Phys. Rev. B* **1998**, *58*, 2207. (d) Ferrari, A. C.; Rodil, S. E.; Robertson, J. *Phys. Rev. B* **2003**, *67*, 155306.
- (10) Kroke, E.; Schwarz, M. *Coord. Chem. Rev.* **2004**, *248*, 493.
- (11) (a) Wang, J.; Miller, D. R.; Gillan, E. G. *Chem. Commun.* **2002**, 2258. (b) Wang, J.; Miller, D. R.; Gillan, E. G. *Carbon* **2003**, *41*, 2031. (c) Wang, J.; Gillan, E. G. *Thin Solid Films* **2002**, *422*, 62. (d) Miller, D. R.; Wang, J.; Gillan, E. G. *J. Mater. Chem.* **2002**, *12*, 2463. (e) Gillan, E. G. *Chem. Mater.* **2000**, *12*, 3906.
- (12) Miller, D. R.; Swenson, D. C.; Gillan, E. G. *J. Am. Chem. Soc.* **2004**, *126*, 5372.
- (13) (a) Riedel, R.; Horvath-Bordon, E.; Nahar-Borchert, S.; Kroke, E. *Key Eng. Mater.* **2003**, *247*, 121. (b) Komatsu, T. *J. Mater. Chem.* **2001**, *11*, 802. (c) Komatsu, T.; Nakamura, T. *J. Mater. Chem.* **2001**, *11*, 474. (d) Komatsu, T. *Macromol. Chem. and Phys.* **2001**, *202*, 19. (e) Komatsu, T. *J. Mater. Chem.* **2001**, *11*, 799. (f) Jurgens, B.; Irran, E.; Senker, J.; Kroll, P.; Muller, H.; Schnick, W. *J. Am. Chem. Soc.* **2003**, *125*, 10288. (g) Lotsch, B. V.; Schnick, W. *Chem. Mater.* **2005**, *17*, 3976. (h) Lotsch, B. V.; Schnick, W. *Chem. Mater.* **2006**, *18*, 1891. (i) Groenewolt, M.; Antonietti, M. *Adv. Mater.* **2005**, *17*, 1789. (j) El-Gamel, N. E. A.; Schwarz, M.; Brendler, E.; Kroke, E. *Chem. Commun.* **2006**, 4741.
- (14) (a) Kroke, E.; Schwarz, M.; Horath-Bordon, E.; Kroll, P.; Noll, B.; Norman, A. D. *New J. Chem.* **2002**, *26*, 508. (b) Horvath-Bordon, E.; Kroke, E.; Svoboda, I.; Fuess, H.; Riedel, R. *New J. Chem.* **2005**, *29*, 693. (c) Horvath-Bordon, E.; Kroke, E.; Svoboda, I.; Fuess, H.; Riedel, R.; Neeraj, S.; Cheetham, A. K. *Dalton Trans.* **2004**, 3900. (d) Traber, B.; Oeser, T.; Gleiter, R.; Goebel, M.; Wortmann, R. *Eur. J. Org. Chem.* **2004**, 4387. (e) Ke, Y.; Collins, D. J.; Sun, D.; Zhou, H.-C. *Inorg. Chem.* **2006**, *45*, 1897. (f) Sattler, A.; Schnick, W. *Z. Anorg. Allg. Chem.* **2006**, *632*, 238.
- (15) (a) Goettmann, F.; Fischer, A.; Antonietti, M.; Thomas, A. *Angew. Chem., Int. Ed.* **2006**, *45*, 4467. (b) Goettmann, F.; Fischer, A.; Antonietti, M.; Thomas, A. *Chem. Commun.* **2006**, 4530.

- (16) Zheng, W.; Wong, N.-B.; Wang, W.; Zhou, G.; Tian, A. *J. Phys. Chem. A* **2004**, *108*, 97.
- (17) (a) Liebig, J. V. *Ann. Pharm.* **1834**, *10*, 1. (b) Gmelin, L. *Ann. Pharm.* **1835**, *15*, 252. (c) Franklin, E. C. *J. Am. Chem. Soc.* **1922**, *44*, 486.
- (18) (a) Pauling, L.; Sturdivant, J. H. *Proc. Nat. Acad. Sci. U.S.A.* **1937**, *23*, 615. (b) Hosmane, R. S.; Rossman, M. A.; Leonard, N. J. *J. Am. Chem. Soc.* **1982**, *104*, 5497. (c) Shahbaz, M.; Urano, S.; LeBreton, P. R.; Rossman, M. A.; Hosmane, R. S.; Leonard, N. J. *J. Am. Chem. Soc.* **1984**, *106*, 2805.

internal temperature of 200 °C over the course of 3 h. Once the heating time had elapsed, the system was cooled to room temperature, the pressure release valve was opened very briefly, and pressurized volatiles were vented into a fume hood. Note that evolved gas pressure was below the detection minimum of the pressure gauge for this reaction scale. In the case of samples isolated and analyzed under inert conditions, the autoclave assembly was disassembled in a glovebox. A visibly porous, fluffy, chocolate-brown powder was isolated from within the beaker. In the case of samples isolated and analyzed under atmospheric conditions, the autoclave assembly was disassembled in ambient laboratory atmosphere after venting. Over the course of several weeks in air, the chocolate-brown air-exposed powder became yellow-tan. The isolated powder yield was 40–50 mg.

Method 2. Inside an argon-atmosphere glovebox, TAH (100 mg, 0.34 mmol) was placed inside a 60 mL custom calorimeter-style, stainless steel reactor (screw top, inner dimensions of 5.4 cm depth \times 3.8 cm width, 5 mm thick walls, and a removable cap with four insulated posts.^{11d} The decomposition reaction was initiated in a hood by briefly (\sim 2 s) passing 20 V across a nichrome filament affixed to two of the posts. This voltage causes the filament to glow orange and quickly reaches temperatures near 500 °C. The internal temperature of the reaction was recorded by a 0.1 mm type K thermocouple that was affixed to the remaining two posts and placed in contact with the precursor, but separated from the heated filament. Note that although this reactor is assembled and closed under inert conditions, the reactor is not airtight; thus, possible exposure to ambient atmosphere is minimized but not eliminated. Once initiated, the reaction is complete within seconds, at which point the reactor was either immediately taken into a glovebox and disassembled where the product was isolated for inert storage and analysis or the reactor was disassembled in air and product isolated. In both cases, a visibly porous, fluffy, chocolate-brown powder was isolated from the reactor. Over several weeks, the chocolate-brown air-exposed powder became yellow-tan. The isolated powder yield was 35–40 mg.

Method 3. Using the same autoclave apparatus as described in Method 1, slow decomposition was achieved by heating 100 mg of TAH in a stepwise fashion to an internal temperature of 100 °C for 1 day, then 150 °C for 1 day, then 170 °C for 1 day, then 220 °C for 1 day, and finally to 250 °C for 1 day. Inert and air-exposed samples from this decomposition were isolated as described above for the Method 1 product isolation. A dark brown powder was isolated, which was neither visibly porous nor fluffy, but was a contained mass at the bottom of the beaker that had an overall morphology reminiscent for the microcrystalline precursor powder. Over the course of several weeks in air, the dark brown air-exposed powder retained its original color. The isolated powder yield was 50–60 mg.

Product Analysis. Thermogravimetric-differential thermal analysis (TG-DTA) was performed on a Seiko ExStar 6300 system under flowing argon. FT-IR absorption spectra were taken with a Nicolet Nexus 670 spectrometer using KBr pellets. Elemental analysis (CHNO) was performed by Desert Analytics, Inc. (www.desertanalytics.com). Powder X-ray diffraction was run on powders affixed to glass slides using a Siemens D5000 diffractometer. Scanning electron microscopy was carried out on a field emission Hitachi S4000 microscope. The densities of the TAH decomposition products were determined using the flotation method with chloroform and bromoform as the solvent mixture. Solid-state ¹³C NMR was obtained at room temperature using a Bruker Avance 600 NMR system (Iowa State University) in both MAS (60 s recycle delay; 15 440 scans) and CP-MAS (5 s recycle delay, 2 ms contact

time, 6000 scans) pulse sequence modes. The samples were loaded into 4 mm rotors that were spun at 10 kHz, and data were referenced to glycine at 176 ppm.

The evolved gases from the rapid decomposition of TAH were measured at room temperature by mass spectrometry using a Stanford Research Systems QMS 300 gas analyzer (survey scans to 300 amu, quantitative scans to 150 *m/z*, 25 points/amu resolution, three scans averaged). Inside an argon atmosphere glovebox, TAH (30 mg, 0.1 mmol) was placed inside a flame-dried 250 mL Schlenk flask. The flask was evacuated to <100 mTorr and backfilled with argon gas three times. Rapid decomposition was performed under argon using a heating mantle heated to 200 °C over the course of 30 min. The flask was isolated from the argon gas manifold immediately following detonation of TAH and cooled to room temperature. The sidearm of the flask was attached to the gas analyzer's sampling capillary via a Tygon tube sleeve. The capillary was evacuated to instrumental background levels (\sim 10⁻⁸ Torr), then the sidearm stopcock was opened and it was positioned in the center of the flask, and the gas analysis was initiated. A control experiment was performed using a flame-dried 250 mL Schlenk flask filled with argon.

UV-visible spectra were obtained from powders spread on filter paper or in MeOH suspensions using an HP 8453 diode-array spectrophotometer equipped with a diffuse reflectance attachment. Samples for fluorescence measurements were prepared by sonicating powders in MeOH to generate a suspension. The suspension was then slowly pipetted onto a warm, silicon wafer atop a heating plate. Slow evaporation of the MeOH produced a film of powder on the silicon surface. The films were affixed to a custom-made aluminum holder with double-sided tape. Fluorescence measurements were performed using a ThermoSpectronic Aminco Bowman Series II luminescence spectrometer with 300 nm excitation and measured at nearly 50° off of the detector normal to reduce scattering radiation.

Results and Discussion

Thermal Stability of 2,5,8-Triazido-s-heptazine (TAH). Initial thermogravimetric-differential thermal analysis (TG-DTA) experiments run under argon at 5–10 °C/min using 5 mg of TAH showed a sharp exothermic event simultaneous with total weight loss at 185 °C. However, upon opening the system, a fluffy powder was visible around the interior, which contradicted the total weight loss recorded by the balance. It was concluded that TAH had decomposed violently enough to blow the majority of the powder out of the sample pan, causing the instrument to register an artificially large weight loss. Upon reducing the TAH mass to <1 mg and slowing the temperature ramp to 2 °C/min, a mass loss of \sim 28% was recorded at 185 °C, which is consistent with the loss of three N₂ per TAH molecule (Figure 2). Further heating of the remaining material resulted in gradual, but complete weight loss by 600 °C. This decomposition was also accomplished more slowly by performing a TG-DTA under isothermal conditions at 150 °C (Figure S1, Supporting Information). This showed that TAH is relatively stable for about 3 h, after which it slowly loses weight over the next 5 h reaching a stable 28% weight loss, again consistent with the loss of three N₂ molecules. We cannot rule out whether some molecular TAH sublimation also occurs during both these fast and slow decomposi-

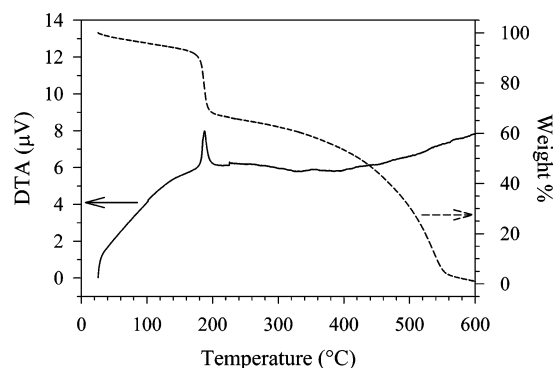
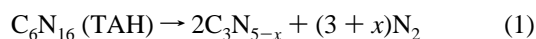


Figure 2. TG-DTA plot for TAH decomposition using a heating ramp of 2 °C/min (argon flow).

tion processes. For example, high-vacuum solid probe mass spectrometry experiments on TAH up to ~350 °C show evidence of parent ion volatility.¹²

The evolved gases from a small-scale (~30 mg) rapidly heated TAH decomposition were analyzed using a residual gas mass spectrometer. The only volatile components observed above the ambient background were significant amounts of N₂ gas (Figure S2). A very small peak is observed that may also correspond to cyanogen, (CN)₂. No other identifiable volatile species up to 300 amu, such as fragments of heptazine, were detected in the gas phase after rapid TAH decomposition. Note that this room-temperature analytical method will only detect fragments with sufficient gas-phase volatility. The evolved gas analysis data are consistent with the proposed thermally initiated decomposition of TAH, as shown in eq 1.



The bulk thermal decomposition of TAH utilizing either a rapidly heated stainless steel autoclave (Method 1) or a rapidly heated filament (Method 2) resulted in isolation of a visibly porous, fluffy, chocolate brown powder. An in-situ thermocouple recorded temperature spikes as high as 180 °C during TAH filament initiated decomposition. In contrast, when a stepwise heating procedure in an autoclave was used (Method 3), the resulting product was a dark brown, nonporous powder that had well-defined facets and edges when viewed with an optical microscope (200× mag). Powder X-ray diffraction showed all products to be amorphous or only very poorly locally ordered with, at best, a broad peak corresponding to carbon–carbon Van der Waals contacts (~3.4 Å), as has been seen in many other nitrogen-rich carbon nitride systems (Figure S3).^{8,10,11}

Table 1 displays the bulk combustion elemental analysis (EA) data for carbon nitride products derived from TAH decomposition using Methods 1–3. There are several noteworthy points to be taken from this data. First, precursor preparation has a measurable effect on product composition as seen by comparing entries A and B. Although the decomposition method was the same and both products were isolated and analyzed under inert conditions, the product obtained from the as-synthesized TAH (entry A) has a relatively lower carbon and higher nitrogen content and

almost no oxygen compared to the CN_x product from the acetone-recrystallized precursor (entry B). We conclude that the increase in carbon and oxygen content seen in entry B relative to A is a result of acetone residue being present in the recrystallized TAH, which is then incorporated into the product during decomposition. This is consistent with NMR data on the TAH precursor powder that show acetone peaks in the ¹³C NMR spectrum at 30.4 (methyl) and 217.1 ppm (carbonyl) and in the ¹H NMR at 2.05 ppm (methyl). The acetone-recrystallized TAH precursor powder that was vacuum-dried at 100 °C has EA values consistent with a formula of C_{6.7}N₁₆H_{1.6}O_{0.7} (or C₆N₁₆·C_{0.7}H_{1.6}O_{0.7}), so some acetone may remain bound to crystallite surfaces, even though no acetone was detected in the bulk crystal structure.¹²

The rapidly synthesized CN_x powder by Method 1 shows some reactivity toward organic solvents and ambient atmosphere that likely passivate unstable bonds in the product. Such exposure may cause surface atoms and other kinetically stable species to react with moisture or abstract hydrogen from solvents and increase relative hydrogen and oxygen contents. Related CN_x materials formed from the slow decomposition of a smaller azide heterocycle, triazido-*s*-triazine (TAT), were similarly sensitive to hydrogen abstraction from solvents and slowly react in ambient air.^{11e} A comparison of Table 1 entries A and C shows that the compositional effect of solvent and atmospheric exposure is more significant than acetone recrystallization effects alone (entry B) but is similar to a combination of acetone recrystallization and air exposure (entry D).

The EA data also show that the type of rapid decomposition method has a minor influence on the bulk product composition as seen by comparing CN_x products from Methods 1 (entry D) and 2 (entries E and F). In contrast, the slower decomposition pathway (Method 3) resulted in CN_x solids with improved stability to air exposure and slightly lower oxygen content when handled under comparable conditions (entries G and H). The improved air stability of the Method 3 products may be due to the slow (non-explosive) decomposition process that allows for increased formation of stable bonds and in situ passivation of reactive bonds. Generally, the more air-sensitive rapidly synthesized CN_x powders changed from a chocolate brown color to a yellow-tan color over the course of nearly a month in air, while the dark brown color of the Method 3 slow decomposition product was unchanged in air over a similar period.

Spectroscopic Analysis of TAH Decomposition Products. The FT-IR spectrum representative of the carbon nitride material generated by either rapid Method 1 or 2 under inert conditions is shown in Figure 3a, while the spectrum for an air-exposed product is shown in Figure 3b. Figure 3c displays the spectrum for the slow Method 3 decomposition product isolated after air exposure. The spectrum of the TAH molecular precursor is shown in Figure 3d. A comparison of inert and air exposed CN_x products shows that a medium intensity, broad vibration near 3300–3500 cm⁻¹ and an N–H bending mode near 1400 cm⁻¹ are significantly more prominent in the air-exposed product's spectrum (spectrum a vs b of Figure 3, see asterisk-marked peaks). These data

Table 1. Summary of Elemental Analysis Data for Various TAH Decomposition Products

TAH preparation	TAH dec description	C wt %	H wt %	N wt %	O wt % ^a	total wt %	formula	
A	as-synthesized	Method 1, Rapid Parr, inert	32.34	1.13	65.55	0.98	100.0	C ₃ N _{5.2} H _{1.3} O _{0.07}
B	acetone recryst	Method 1, Rapid Parr, inert	41.06	1.03	47.67	9.22	98.98	C ₃ N _{3.8} H _{1.1} O _{0.64}
C	as-synthesized	Method 1, Rapid Parr, inert toluene wash, air exposed	33.74	2.13	48.32	14.92	99.11	C ₃ N _{3.6} H _{2.2} O _{0.97}
D	acetone recryst	Method 1, Rapid Parr, air exposed	34.96	1.48	49.54	14.31	100.3	C ₃ N _{3.8} H _{1.6} O _{0.95}
E	acetone recryst	Method 2, filament, inert	34.62	1.40	47.46	15.51	98.99	C ₃ N _{3.8} H _{1.6} O _{1.1}
F	acetone recryst	Method 2, filament, air exposed	32.15	1.99	47.51	17.32	98.97	C ₃ N _{3.8} H _{2.2} O _{1.2}
G	acetone recryst	Method 3, Stepwise Parr, inert	35.00	2.71	54.56	7.27	99.54	C ₃ N _{4.1} H _{2.8} O _{0.48}
H	acetone recryst	Method 3, Stepwise Parr, air exposed	33.76	1.83	54.99	7.62	98.20	C ₃ N _{4.2} H _{1.9} O _{0.51}

^a Calculated by difference for entry A, all other samples were analyzed for oxygen content

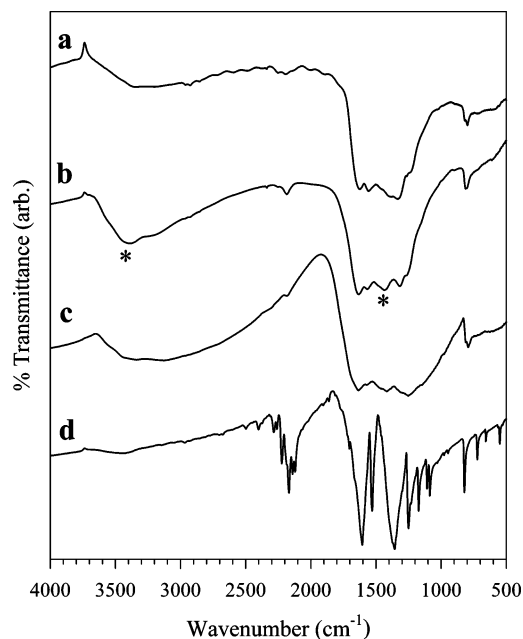


Figure 3. FT-IR comparison of CN_x products from (a) rapid decomposition of TAH via Method 1 under inert conditions, (b) rapid decomposition of TAH via Method 1 after air exposure, (c) slow decomposition of TAH via Method 3 after air exposure, and (d) the TAH precursor. The asterisks indicate N–H vibrational regions.

suggest that OH and NH bonds are formed through reaction with ambient moisture, leading to generally higher hydrogen and oxygen contents of the air-exposed samples and suggesting that the reactive species in the as-synthesized CN_x are likely nitrogen-based, such as nitrenes, strained heterocyclic rings, or diazonium residues. The distribution of C=N and C–N vibrational modes in the 1200–1700 cm⁻¹ region is different between the inert and air-exposed products, with slightly stronger C–N modes near 1300 cm⁻¹ relative to the C=N modes near 1550 cm⁻¹.

Upon air exposure, the relative intensity of these C–N and C=N regions is reversed, which may be due to some C–N (or N–N) bond cleavage during air exposure. The air-exposed product also shows a more intense peak near 2190 cm⁻¹ that could arise from the formation of imine (C=NH), nitrile (–C≡N), or diimide (–N=C=N–) surface structures. The peak at ~810 cm⁻¹ present in all spectra and is a characteristic ring breathing mode seen in both triazine and heptazine precursors (cf., Figure 3d) indicating that conjugated ring structures remains intact in the CN_x products. The CN_x spectral features have much in common with other extended C–N network materials derived from triazine and heptazine precursors, particularly with respect to the broad

Table 2. Comparison of Carbon NMR Chemical Shifts for Heptazine Systems (C₆N₇)X₃

X in (C ₆ N ₇)X ₃	C (internal)	C (external)	ref
Solution State			
H	159.7	171.6	18b
Cl	158.2	175.0	14a
N ₃	158.7	171.4	12
O ⁻ M ⁺	159.1–161.0	169.3–171.5	14c
M = Li, Na, K, Rb, Cs			
N(Et) ₂	155.0	162.4	14d
Solid State ^a			
NH ₂	155.1, 156.0	164.3, 166.4	13f
CN _x from TAH	156.0 (153.7)	163.7 (164.6)	this work

^a CP-MAS data shown with MAS data in parentheses.

overlapping peaks in the C–N bonding region and prevalent N–H vibrational modes.^{8,11,13}

The FT-IR spectrum of the air-exposed product via Method 3 is shown in Figure 3c. This spectrum possesses many of the same features seen in Figure 3b with several key differences. The broad peak in the 3300–3600 cm⁻¹ region shows less intensity from 3500 to 3600 cm⁻¹, suggesting that OH stretching is not as prominent because of its lower moisture reactivity. The spectrum also displays significant absorption in the 1000–1200 cm⁻¹ region possibly resulting from the presence of increased N–N bonding, consistent with higher nitrogen content. There is also broadening in the 1200–1700 cm⁻¹ region perhaps due to the solid's extended bonding being greater or more heterogeneous as compared to the CN_x products generated by rapid TAH decomposition.

Solid-state ¹³C NMR has significant utility in the analysis of local carbon environments in disordered CN_x materials. Symmetric triazine (C₃N₃) molecular precursors and triazine-based CN_x solids generally show single ¹³C NMR peaks with chemical shifts that are characteristic of carbon bonded to external species such as N–H or other rings (δ ≈ 160–170 ppm).¹⁹ From the TAH structure in Figure 1, it is clear that a heptazine-based network should show two distinct ¹³C shifts, one for the internal/junctional carbon (bonded to three heptazine nitrogens including the central nitrogen) and another for the external carbon (bonded to N₃ in TAH). Several prior studies on heptazine in molecular and extended networks give us clear data on the expected chemical shifts for these two carbon sites. Table 2 compares the data for the rapidly decomposed TAH product with several reported heptazine structures. The two NMR peaks determined for our CN_x material from TAH decomposition are consistent

(19) Katritzky, A. R.; Oniciu, D. C.; Ghiviriga, I.; Barcock, R. A. *J. Chem. Soc., Perkin Trans. 2* **1995**, 785.

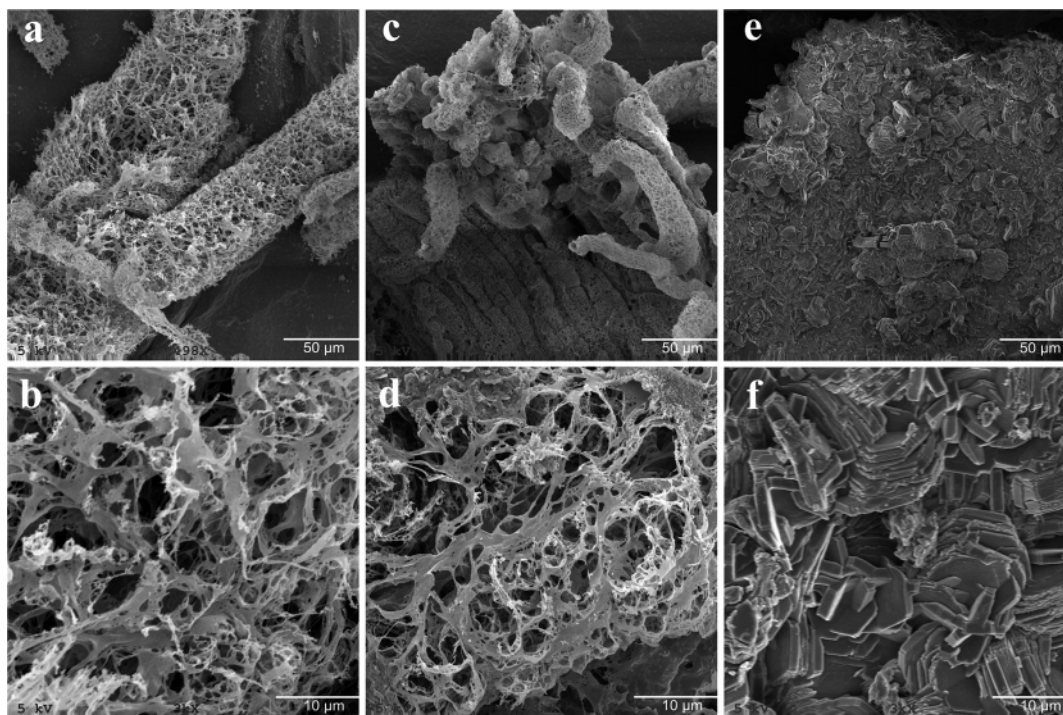


Figure 4. SEM images of TAH decomposition products generated by (a,b) Method 1 (rapid autoclave), (c,d) Method 2 (filament), and (e,f) Method 3 (stepwise autoclave).

with a local heptazine structure where the external carbon is in closer proximity to hydrogen species, as indicated by increased peak intensity for the external carbon using CP-MAS versus MAS analysis (see Figure S4).

CN_x Product Morphology and Microstructure. The rapid versus slow (non-explosive) TAH decomposition routes do not result in significantly different product nitrogen content; however, they produce CN_x powders with significantly different product morphologies. Scanning electron microscopy (SEM) images of CN_x powders from rapid decomposition of TAH via Methods 1 and 2 reveal a microstructure that is visibly very porous and consistent with the rapid evolution of byproduct gases during pyrolysis (Figure 4a–d). Higher-resolution images show that regions of the particulate structure have a torn, jagged appearance. This morphology is reminiscent of a gas-blown, polymeric foam and consistent with the rapid mass loss observed by TG-DTA (Figure 2) that is primarily N₂, as shown by mass spectrometry evolved gas analysis. This gas evolution and network formation process is most likely complete within a second or two, which is consistent to visual observations during the evolved gas analysis experiment.

In sharp contrast, even at low magnification, the CN_x material derived from the stepwise pyrolysis of TAH (Method 3) shows clear, crisp edges and rodlike structures (Figure 4e). Higher magnification of this product reveals a morphology that appears to be a microcrystalline powder with faceted $\sim 1 \mu\text{m}$ long rods and $\sim 10 \mu\text{m}$ wide plates (Figure 4f). Regardless of the apparent crystal faceting, powder X-ray diffraction shows this sample to be essentially amorphous, consistent with most previous reports on nitrogen-rich CN_x network materials. Since the TAH precursor was used as a microcrystalline powder, the above results support

the proposition that the slow decomposition of TAH occurs in such a gradual manner (as observed by TG-DTA, Figure S1) that the microcrystals of the TAH precursor did not lose their overall crystallite morphology when N₂ gas is liberated. During decomposition, the crystals are reduced in volume, resulting in an amorphous, but well-shaped, carbon nitride material. An SEM image of the starting TAH crystals could not be obtained due their facile decomposition in the electron beam; however, an optical microscope examination shows the precursor powder is composed of short, needlelike microcrystallites having a prismatic, hexagonal crystal habit, consistent with the morphologies seen in Figure 4e–f.

In light of the morphology differences, density measurements were taken for selected samples from different precursor batches and different decomposition methods. The result was an average density value of $1.52 \pm 0.05 \text{ g/cm}^3$. The surprisingly small standard deviation reflects that, within measurement errors, the densities of the CN_x solids are very similar, regardless of TAH decomposition method. This result supports the idea that the local chemical structure of the various TAH decomposition products is comparable and the product morphology is affected primarily by the rate of gas evolution. This density value is lower than graphitic carbon (2.3 g/cm^3) and higher than polymers such as polyethylene ($\sim 0.9\text{--}1 \text{ g/cm}^3$), but it is consistent with values we measured for nitrogen-rich CN_x solids synthesized from triazine precursors.^{11d}

Thermal Stability of TAH Precursor and Derived CN_x Powders. The results for rapid decomposition of TAH are very different than those for rapid decomposition of its smaller single heterocyclic ring analog, triazido-*s*-triazine [TAT, C₃N₃(N₃)₃, C₃N₁₂]. The rapid decomposition of TAT results in complete loss of nitrogen and formation of graphite

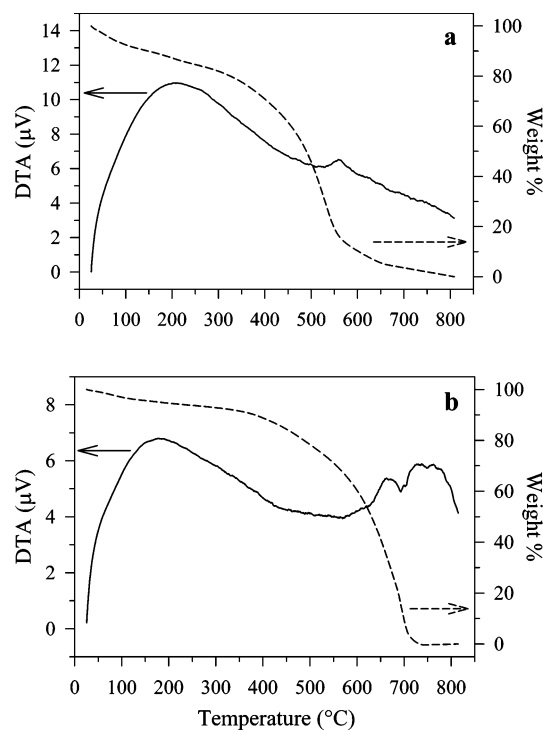


Figure 5. TG-DTA plots for TAH Parr autoclave decomposition products generated via (a) rapid heating (Method 1) and (b) slow, stepwise heating (Method 3).

nanoflakes^{11e} or carbon nanotubes.²⁰ Hence, under the conditions reported here, the *s*-heptazine provides a more stable precursor core that is less prone toward ring opening and nitrogen loss. Theoretical studies of the TAH and TAT molecules predict that $n-\pi^*$ or $\pi-\pi^*$ stabilization energy in *s*-heptazine is ~ 40 kJ/mol greater than for *s*-triazine, even though the *gas phase* molar heat of formation of TAH is predicted to be higher (+1250 kJ/mol) than that of the smaller TAT molecule (+914 kJ/mol).¹⁶ On a weight or carbon atom basis, TAH (4.2 kJ/g or 208 kJ/mol C) is slightly more thermodynamically stable than TAT (4.9 kJ/g or 305 kJ/mol C) in the gas phase. It has been calculated that CN_x materials consisting of *s*-heptazine repeat units should be more thermodynamically stable than those derived from *s*-triazine.^{14a} Solid TAH is significantly less shock sensitive than TAT, possibly due to additional stabilization from solid-state $\pi-\pi$ stacking interactions that are not taken into account in the theoretical gas-phase heat of formation values.¹² The solid TAH decomposition process is sufficiently different from the TAT molecule's full degradation that TAH precursor's degradation stops at a kinetically stabilized conjugated heptazine CN_x intermediate versus completely decomposing to carbon and nitrogen gas.

Despite their different morphologies, the thermal stability of CN_x materials from rapid and slow TAH decomposition are similar. Figure 5a shows a representative TG-DTA for the rapidly decomposed material produced via Methods 1 or 2, which behaves as a typical nitrogen-rich CN_x solid.^{8,10,11} The sample is relatively stable up to 500 °C where it begins to break apart and lose mass. Similar CN_x materials are

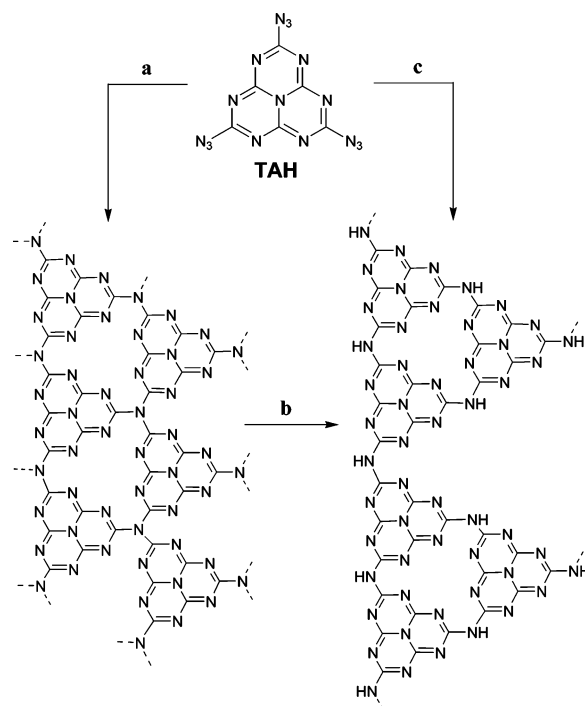


Figure 6. Structural speculation for TAH CN_x products resulting from thermal decomposition (a) under inert conditions with minimal acetone in precursor, (b) under conditions in (a) followed by air exposure, or (c) under inert conditions with acetone present in the precursor.

known to decompose/evaporate by ~ 600 °C and recondense as CN_x structures at ~ 400 °C.^{11a} Solid probe mass spectrometry on the rapidly decomposed TAH product heated to 350 °C did not detect volatile fragments up to 500 amu. The main mass losses in Figure 5 are consistent with CN_x network breakdown and a broad endothermic peak is simultaneously observed with this mass loss, consistent with gradual decomposition and/or volatilization. The TG-DTA for the stepwise decomposed product (Method 3) is shown in Figure 5b and illustrates that the solid has thermal stability similar to the rapidly synthesized products. Interestingly, mass loss begins ~ 50 °C higher for the stepwise versus rapidly decomposed products, supporting earlier IR speculation that the slower TAH decomposition leads to a more thermodynamically stable CN_x structure formed by slowly annealing out defects and improving extended bonding in the solid structure.

Optical Properties of CN_x Powders. The TAH precursor absorbs UV light with major peaks at 275 and 295 nm and shows broad photoluminescence near 430 nm.¹² TAH-derived CN_x powders show an absorption peak at 300 nm and a broad absorption over the entire visible range, consistent with their yellow-tan to chocolate-brown appearance; however, no photoluminescence was obtained for any of the TAH-derived CN_x powders. While luminescence from molecular heptazines is frequently observed,^{14,18b,c} defects in extended solids may quench emission from locally conjugated substructures that retain the heptazine $n-\pi^*$ or $\pi-\pi^*$ orbital transitions.

Structural Possibilities for CN_x Powders. The structure drawn in Figure 6 (left), showing *s*-heptazine cores bridged by tertiary nitrogens, is a possible representation of the CN_x products isolated under inert conditions after TAH decom-

(20) Kroke, E.; Schwarz, M.; Buschmann, V.; Miehe, G.; Fuess, H.; Riedel, R. *Adv. Mater.* **1999**, *11*, 158.

position where minimal acetone or moisture is present. Acetone impurities or air exposure may alternately produce hydrogenated structures such as that shown in Figure 6 (right). This structure accounts for the N–H stretching and bending, as well as the reduced intensity of C–N bonding, as the tertiary nitrogens react to form secondary amines. Increased oxygen content may also produce some C–OH components that could engage in local keto–enol tautomerization with the ring nitrogens. While the heptazine core retention was established by solid-state NMR, the long-range connections are likely heterogeneous and may contain a mix of bridging and terminal nitrogen species.

Many research groups, including ours, have previously proposed structures of carbon nitride materials based solely on *s*-triazine building blocks.^{2,8,11} In these efforts, the starting materials were *s*-triazine derivatives, so the proposed product CN_x structures are reasonable. Extended heptazine-based CN_x solids derived from the decomposition of TAH show significant thermal and spectral similarities to previously reported materials derived from *s*-triazines, suggesting that carbon nitride materials derived from *s*-triazine precursors may also be largely composed of *s*-heptazine substructures. This structural speculation has several precedents; for example, a 1922 review article described a thermal deammonation pathway where guanidine condenses to melamine [$C_3N_3(NH_2)_3$] then to heptazine-based species such as melem [$C_6N_7(NH_2)_3$] or melon ($[-C_6N_7(NH_2)NH-]_n$).^{17c} This decomposition process was recently defined in much more spectroscopic and structural detail and used to grow heptazine-based structures.^{13f–i} Researchers have also proposed triazine to heptazine conversions may occur during the thermal precursor conversion processes to form CN_x

structures.^{13h} We are currently re-examining the local structures of triazine-based carbon nitrides to determine if they contain clearly identifiable heptazine substructures.

Conclusions

Triazido-*s*-heptazine (TAH, C_6N_{16}) is an effective, energetic single-source precursor for the synthesis of nitrogen-rich CN_x ($x \approx 1.2–1.7$) network materials. The surprising thermal stability of the TAH azide precursor enabled CN_x material to be generated through rapid or slow, stepwise thermal decomposition routes. These different routes yield products with similar chemical and thermal properties, but markedly different morphologies. Rapid decomposition yields powders with a porous, spongelike appearance, while slow decomposition results in faceted, amorphous monoliths. Spectroscopic evidence is consistent with local conjugated structures based on interconnected *s*-heptazine rings, leading to thermally robust nitrogen-rich CN_x extended materials.

Acknowledgment. The Army Research Office (DAAD19-03-1-0274) and National Science Foundation (CHE-0407753) are gratefully acknowledged for partial financial support. Shu Xu (Iowa State University) and Darrell Eyman (University of Iowa) are acknowledged for acquisition of the solid-state NMR data and use of an SRS mass analyzer, respectively.

Supporting Information Available: TG-DTA data for isothermal heating of TAH at 150 °C, followed by ramping to 1000 °C, evolved gas mass spectra for volatile TAH decomposition byproducts, and XRD data and ¹³C NMR spectra for rapidly synthesized CN_x product. This material is available free of charge via the Internet at <http://pubs.acs.org>.

IC061296Y